DAN LANGLEY 24p.

WASHINGTON UNIVERSITY
DEPARTMENT OF PHYSICS
LABORATORY FOR ULTRASONICS
St. Louis, Missouri 63130

IN-30262

"Quantitative Non-Destructive Evaluation of Composite Materials Based on Ultrasonic Wave Propagation"

Semiannual Progress Report: March 15, 1986 - September 14, 1986

NASA Grant Number: NSG-1601

Principal Investigator:

Dr. James G. Miller
Professor of Physics

The NASA Technical Officer for this grant is:

Dr. Joseph S. Heyman
NASA Langley Research Center
Hampton, Virginia

I. INTRODUCTION

The research described in this Progress Report is aimed toward extension of the application and interpretation of specific ultrasonic nondestructive evaluation techniques. The first section of this Report deals with the application of Kramers-Kronig or generalized dispersion relationships. The second section reports on our progress on an improved determination of material properties of composites inferred from elastic constant measurements.

II. KRAMERS-KRONIG RELATIONSHIP

Previous research has made use of generalized Kramers-Kronig relationships.[1,2] One goal of our continuing research is to extend the generalized dispersion relationships to inherently inhomogeneous media such as composites. Experiments based on the technique of ultrasonic phase spectroscopy introduced by Sachse and his colleagues[3] have been carried out to evaluate the potential of this approach as a method for local characterization of material integrity. (A portion of the funding for this research was derived from a NASA Graduate Student Research Fellowship awarded to Michael S. Hughes.)

A. THEORETICAL BACKGROUND

Kramers-Kronig or generalized dispersion relationships, are useful in many areas of physics. Our studies are based on the following form of these equations,

$$K_1(\omega)-K_1(\infty) = \frac{2}{\pi}\int_0^\infty \frac{\omega' K_2(\omega')}{\omega'^2-\omega^2}\,d\omega', \tag{1}$$

$$K_2(\omega) = -\frac{2\omega}{\pi}\int_0^\infty \frac{K_1(\omega')-K_1(\infty)}{\omega'^2-\omega^2}\,d\omega' \tag{2}$$

where $K_1(\omega)$ and $K_2(\omega)$ are the real and imaginary parts, respectively, of the dynamic compressibility $K(\omega)$. Writing the ultrasonic wave vector as $\omega/C(\omega)+i\alpha(\omega)=k$, we identify $C(\omega)$ as the phase velocity and $\alpha(\omega)$ as the attenuation coefficient for the wave inside a specimen, as observed in transmission measurements. The effect of a specimen on the incident wave can be represented by a phenomenological compressibility $K(\omega)$ obeying Eqs. (1) and (2), which can be used to define the relationship between attenuation and dispersion. To do this we use the dispersion relation for acoustic waves which we write as

$$k^2 = \omega^2\rho_0 K(\omega). \tag{3}$$

This leads to the following pair of equations,

$$K_1(\omega)=\frac{1}{\rho(C(\omega))^2}-\frac{\alpha(\omega)^2}{\rho\omega^2}. \tag{4}$$

and

$$K_2(\omega)=2\frac{\alpha(\omega)}{\rho\omega C(\omega)}, \tag{5}$$

where ρ is the density of the material in which the wave is propagated. In principle the dispersion at a specified frequency can be computed from a knowledge of the attenuation at all frequencies by using Eqs. (2), (4) and (5). This computation would require the solution of an integral equation involving $\alpha(\omega)$ and $C(\omega)$. A closed form answer for $C(\omega)$ in terms of $\alpha(\omega)$ seems unlikely. Conversely, if the dispersion is known at all frequencies, the attenuation at any specific frequency could be computed in principle from Eqs. (1), (4) and (5). However, for similar reasons this approach does not seem attractive.

It is possible to circumvent these mathematical difficulties by using an approximation to the integrals in Eq.(1) and Eq.(2). Previous Reports have focused on experimental tests of a local approximation to these equations. Assuming that the attenuation and dispersion are sufficiently small and change slowly enough over the frequency range of interest, we have shown in previous Progress Reports that

$$\alpha(\omega)\approx\frac{\pi\omega^2}{2C_0^2}\frac{d}{d\omega}C(\omega) \tag{6}$$

$$\frac{1}{C(\omega_0)}-\frac{1}{C(\omega)}\approx\frac{2}{\pi}\int_{\omega_0}^{\omega}\frac{\alpha(\omega')}{\omega'^2}d\omega' \tag{7}$$

where ω_0 is some convenient reference frequency.

Experimental evidence indicates that for some materials of interest the attenuation coefficient can be described approximately by the relation $\alpha(\omega)=\beta\omega$. This observation combined with equation (7) leads to the following approximate relationship between $\alpha(\omega)$ and $C(\omega)$,

$$\Delta C(\omega) = C(\omega)-C_0 \approx \frac{2C_0^2}{\pi}\beta\ln(\frac{\omega}{\omega_0}). \tag{8}$$

A significant umber of approximations are required to derive Eq.(8). As described our the September 1985 to March 1986 Progress Report a more direct test of the local approximation can be based on the equation

$$K_2(\omega) \approx -\frac{\pi}{2}\omega\frac{dK_1(\omega)}{d\omega}. \tag{9}$$

Tests of this form of the local approximation are the subject of the first section of this report.

B. EXPERIMENTAL METHODS

Data are acquired in the time domain using a Tektronix 2430 digital sampling oscilliscope. Data analysis is based on the recently developed ultrasonic phase spectroscopy technique.[3] This method has been described in detail in our Progress Report covering September 1985 to March 1986. It provides the phase and magnitude of a pulse which has propagated through an experimental specimen.

The phase data are used to compute the phase velocity of sound, $C(\omega)$, in the specimen. This analysis is described in detail in the Report cited above.

The magnitude spectrum is used for a qualitative evaluation of the data and to compute the attenuation coefficient as a function of frequency. During the current reporting interval a new procedure for the measurement of attenuation has been implemented in this Laboratory. The geometry used for this procedure is depicted in Fig.(1) where the transmission coefficients at each water-sample and sample-water interface are shown. Data from the front wall reflection are used together with the reference trace data to compute the reflection coefficients as a function of frequency using the formula

$$R_{w\rightarrow s}(\omega) = \frac{M_{fw}(\omega)}{M_r(\omega)} \tag{10}$$

where $M_{fw}(\omega)$ is the magnitude of the frontwall reflection at frequency ω and $M_r(\omega)$ is the magnitude of the reference trace at frequency ω . In practice the reflection coefficient $R_{w\rightarrow s}(\omega)$ is nearly constant over the bandwidth of the apparatus. However, this observation, which is certainly true for materials exhibiting modest attenuation, may not hold in certain composites which exhibit significant attenuation and dispersion.

This reflection coefficient may also be rewritten in terms of physical parameters which characterize the water and the specimen. In terms of characteristic impedances, the particle velocity reflection coefficient $R^u_{1\rightarrow 2}$ and transmission coefficient $T^u_{1\rightarrow 2}$ for particle pressure wave going from medium 1 to medium 2 are

$$R^u_{1\rightarrow 2} = \frac{Z_1 - Z_2}{Z_1 + Z_2} \tag{11}$$

and

$$T^u_{1\rightarrow 2} = \frac{2Z_1}{Z_1 + Z_2} \tag{12}$$

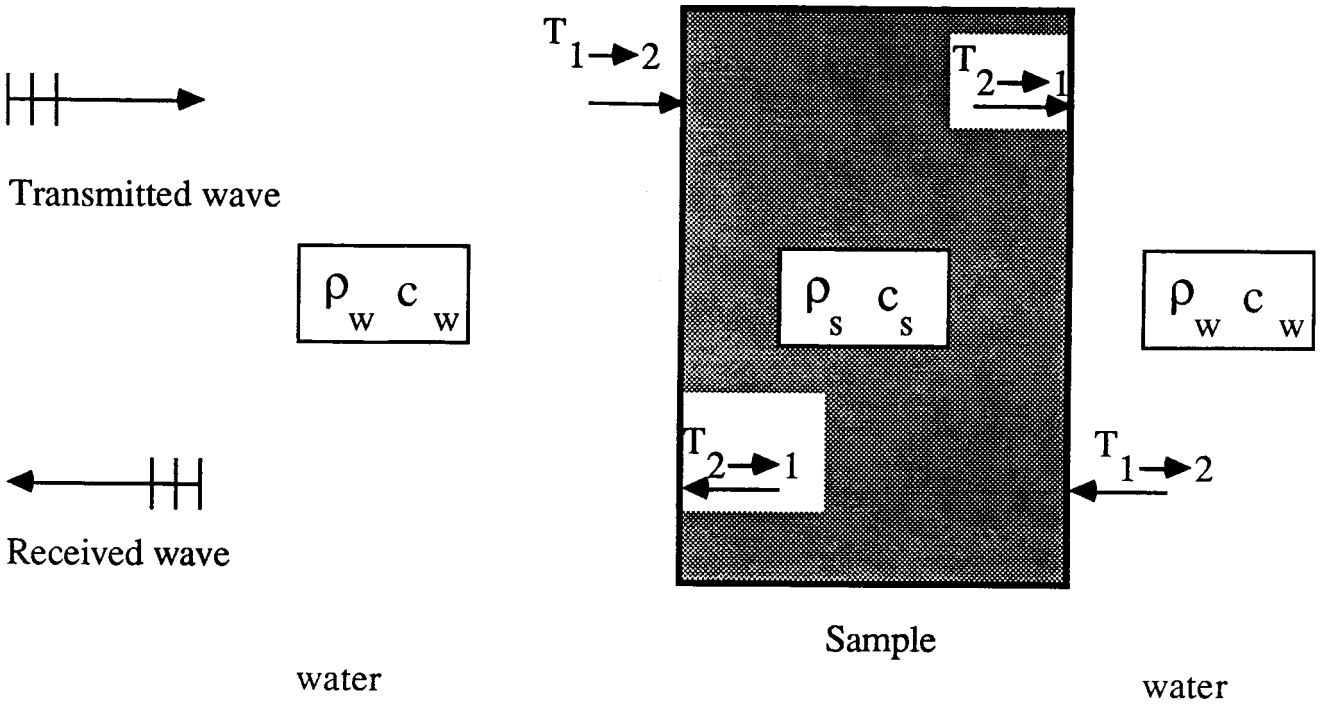

Figure 1 - Diagram of water-sample interfaces encountered by a sound pulse during acquisition of a sample trace. The density of sample is denoted by ρ_s and the density of water by ρ_w . The velocity of sound in the sample is denoted by C_s and in water by C_w .

where Z_1 is the characteristic impedance of medium 1 and Z_2 is the characteristic impedance of material 2. The corresponding pressure reflection and transmission coefficients are

$$R^{p}_{1\to 2} = \frac{Z_2 - Z_1}{Z_1 + Z_2} \tag{13}$$

and

$$T^{p}_{1\to 2} = \frac{2Z_2}{Z_1 + Z_2} \tag{14}$$

From Eqs.(11) thru (14) one obtains the power reflection and transmission coefficients,

$$R^{power}_{1\to 2} = R^{p}_{1\to 2} * R^{u}_{1\to 2} = -\frac{(Z_1 - Z_2)^2}{(Z_1 + Z_2)^2} \tag{15}$$

and

$$T^{power}_{1\to 2} = T^{p}_{1\to 2} * T^{u}_{1\to 2} = \frac{4Z_1 * Z_2}{(Z_1 + Z_2)^2}, \tag{16}$$

where the minus sign in Eq.(15) indicates power flow in the negative direction with respect to the incident pulse. Typical values of these coefficients are shown in Table 1.

For our purposes material one will be taken to be water and material two will represent the sample. From Fig.(1) we see that

$$A_f(\omega) = T_{w\to s} T_{s\to w} T_{w\to s} T_{s\to w} A_i(\omega) \tag{17}$$

where $A_i(\omega)$ is the initial, or uncompensated, magnitude and $A_f(\omega)$ is the final, or compensated, magnitude. Equation (17) may be rewritten as

$$A_f(\omega) = [T_{w\to s} T_{s\to w}]^2 A_i(\omega). \tag{18}$$

An inspection of Eqs.(12) and (14) reveals that Eq.(18) reduces to

$$A_f(\omega) = \left[\frac{4Z_w Z_s}{(Z_w + Z_s)^2}\right]^2 A_i(\omega). \tag{19}$$

independent of whether one is using the particle velocity or the pressure transmission coefficients. We further note that using either Eq.(11) for the particle velocity reflection coefficient or Eq.(13) for the pressure reflection coefficient one can write

$$1 - R^2_{w\to s} = 1 - \left[\frac{Z_w - Z_s}{Z_w + Z_s}\right]^2 = \frac{4Z_w Z_i}{(Z_w + Z_s)^2}. \tag{20}$$

Consequently we have,

Material	Characteristic Impedance gm /cm ^{2}sec	Particle Velocity		Pressure		Power	
		Reflection Coefficient	Transmission Coefficient	Reflection Coefficient	Transmission Coefficient	Reflection Coefficient	Transmission Coefficient
Lexan	1.5	-0.25	0.75	0.25	1.25	-0.06	0.94
Lucite	3.2	-0.36	0.64	0.36	1.36	- 0.13	0.87
Polyethylene	1.8	-0.09	0.97	0.09	1.09	-0.01	0.99
Graphite-Epoxy (uniaxial) perpendicular to fibers	3.1	-0.35	0.65	0.35	1.35	-0.12	0.88
Graphite-Epoxy (uniaxial) parallel to fibers	10.8	-0.76	0.24	0.76	1.76	-0.57	0.43
Graphite-Epoxy (Quasi-Isotropic) perpendicular to fibers	3.6	-0.43	0.57	0.43	1.43	-0.19	0.81

Table 1 - Ultrasonic parameters for various materials of interest. The reflection and transmission coefficients were computed for a sample-water interface assuming the characteristic impedance of water to be 1.5 gm/ cm^2 sec

$$A_f(\omega) = [1-R_{w\rightarrow s}(\omega)]^2 A_i(\omega) \qquad (21)$$

which gives the compensated magnitude in terms of the uncompensated magnitude for either the particle velocity or pressure.

Once the compensated magnitude $A_f(\omega)$ is known, a log subtraction technique is used to compute the attenuation using the magnitude data. It is important to note that the positions of the frontwall of the sample and the stainless steel reflector should be the same at the time of acquisition of both the frontwall reflection data and the reference data. The correct configurations are shown in Fig.(2). The top of this figure shows the placement of transducer and the stainless steel reflector during acquisition of a pulse which propagates through water path only. These data are used as a reference trace to remove instrumental phase shifts and to compute $A_i(\omega)$. Henceforth this will be referred to as the reference pulse. The middle of this figure shows placement of sample, reflector and transducer during acquisition of a pulse which is used together with the reference to compute the phase velocity of sound in the sample. The trace acquired in this configuration will be referred to as the sample trace. The bottom portion of the figure shows sample placement during acquisition of a trace which is used to compute transmission coefficients of the sample. This trace will be referred to as the frontwall reflection trace or the frontwall reflection.

During data acquisition it is essential that these data traces be obtained with the specimen and reflector placed as shown. Failure to do so may produce incorrect estimates of sample attenuation. This observation is illustrated by the following example. A sample of uniaxial graphite-epoxy was insonified at incidence parallel to the fibers. Sample thickness was 3cm so that the distance between the frontwall of the sample and the front of the stainless steel reflector was approximately 3.5cm during acquisition of the sample trace. The relative positions of the transducer, sample and reflector were as shown in the middle of Fig(2). However, during acquisition of the frontwall reflection the sample was positioned as shown in the middle of Fig.(2), not in the position shown in the bottom of Fig.(2).

The outcome of this measurement is shown in Fig.(3a). The apparent attenuation (signal loss) exhibits a bizarre behavior. This incorrect result arises because of the use of an inappropriate estimate of the reflection coefficient. The ultrasonic beam varies substantially as a function of distance from the transducer. If traces acquired at different distances from the transducer are used in the same computation this effect can produce an apparent attenuation that has little connection with the physical properties of the specimen under study. The result of the correct measurement procedure is shown in Fig.(3b)

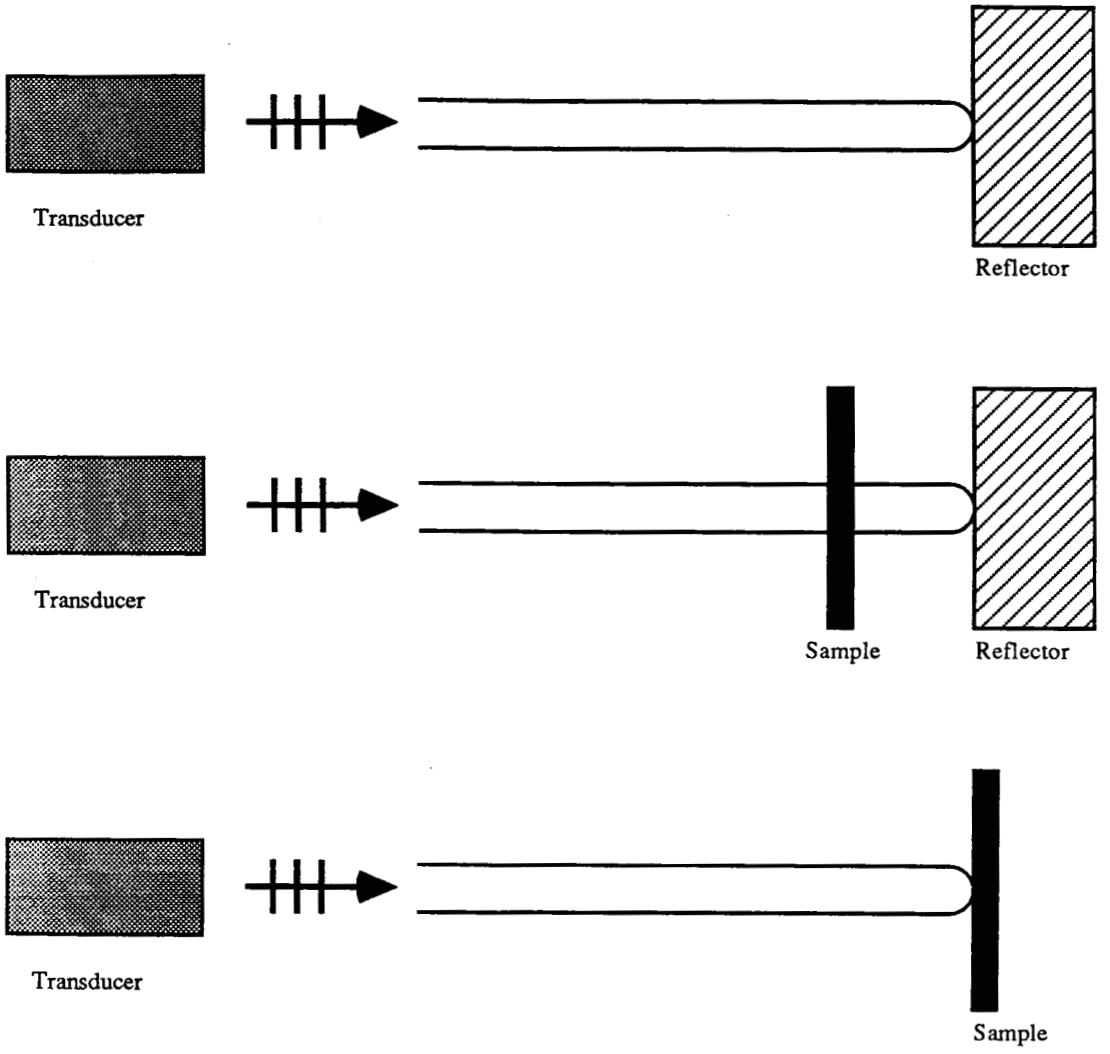

Figure 2 - Diagram indicating the placement of sample and reflector during acquisition of reference trace (top), sample trace (middle) and sample frontwall reflection (bottom)..

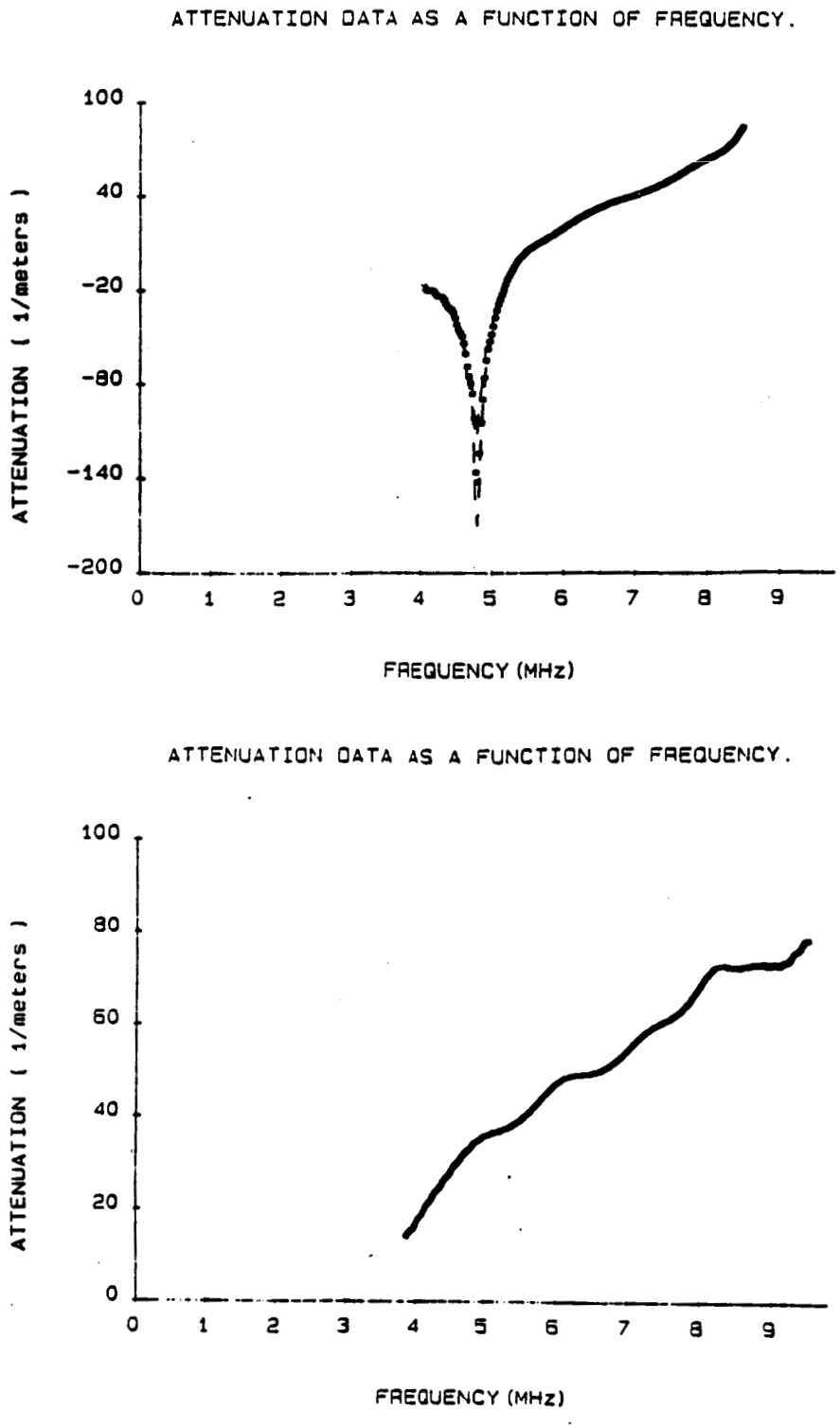

Figure 3 - The top curve shows an incorrect estimate of attenuation in a 3cm specimen of graphite-epoxy. This graph illustrates the result of incorrect placement of frontwall of sample during acquisition of a frontwall reflection trace. The bottom graph shows the correct attenuation data.

in which the relative placements were as shown in Fig.(2).

The results to be discussed in the next section were estimated from the average of five data sets acquired in the time domain. Each of these time domain data sets, in turn, were computed from the average of 5 Tektronix 2430 traces with the oscilliscope set to perform 256 averages internally before outputing the data. This procedure was used to obtain all of the graphs presented in Section I of this report.

One additional methodological consideration concerns traces acquired from thin samples. These frequently contain large specular echoes from both the front and back walls of the sample. If these echoes are included in the segment Fourier transformed the resulting phase and magnitude data are hopelessly corrupted. Thus these echoes must be removed from sample data traces before data analysis can begin. This calls for some type of windowing of the data. In thin samples the choice of window position is much more difficult than it is in a thicker sample.

C. RESULTS

Data collected as described above were used to compute $K_1(\omega)$ and $K_2(\omega)$ via Eqs. (4) and (5). The experimentally measured values of $K_1(\omega)$ were then used in conjunction with Eq.(9) to obtain a local approximation of the values of $K_2(\omega)$. The result of this calculation for a 6.64mm graphite-epoxy composite specimen insonified at perpendicular incidence to the fibers is shown in Fig.(4). In this figure the local approximation, Eq.(9), is represented by diamonds. The crosses represent the result of direct experimental measurement. Standard errors for the local approximation are represented by the two dashed lines. The relatively large magnitude of these errors may be attributed to the fact that computation of the local approximation calls for the differentiation of noisy data. This point is discussed in detail in our Progress Report covering the period from September 1985 to March 1986. We note that the two estimates agree to within the error bars of the local approximation and that the agreement is best at the center of the bandwidth of the apparatus (5.5MHz). It is also important to point out that this sample is thin enough to require the removal of front and backwall reflections from the time domain traces before the data may be Fourier transformed. As described in the Methods section this may be accomplished by use of an appropriate window function. The position of this window is chosen during the course of the data analysis and strongly effects it's outcome. This point is supported by comparision of Fig.(4) of the present Progress Report with Fig.(8) of our Progress Report covering the period from September 15, 1985 to March 14, 1986. Both graphs were obtained from the same time-domain traces. The only difference between the two analyses used to obtain these results is the choice of

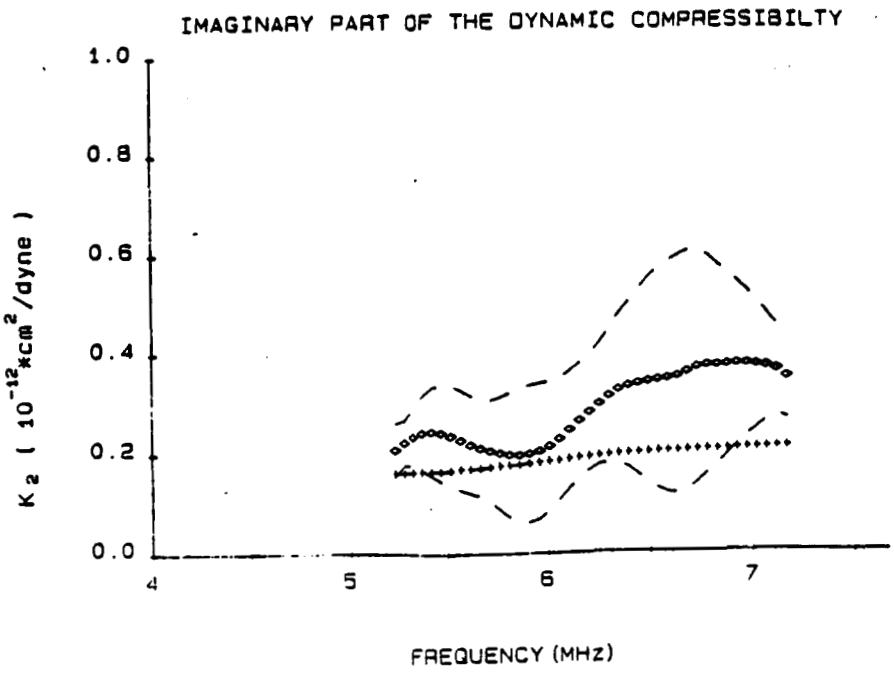

Figure 4 - Comparison of two estimates of $K_2(\omega)$. Experimental data are represented by crosses. The local approximation, Eq.(9), is represented by diamonds. These data were collected from a specimen of graphite-epoxy insonified at incidence perpendicular to the fibers. The error bars shown are those of the local approximation. The sample thickness is 6.64mm.

window position. Figure 4 of this Report shows the outcome of a more appropriate choice for the window position.

A similar study was performed for the specimen of graphite-epoxy 3cm. in thickness insonified at perpendicular incidence to the fibers. Figure (5) shows the comparison of the prediction of Eq.(9) with experiment. The graph in panel a) shows the value obtained using the local approximation with standard errors represented by the two dashed lines. In panel b) the values of $K_2(\omega)$ obtained directly from experimental data are presented with dashed lines to represent the standard errors. In the center of the useful bandwidth the two estimates agree to within the error bars of the direct measurement.

In future research we will investigate dispersion in composite materials using the modified spectroscopy method described above. We will evaluate the range of applicability of the local relationships in these inherently inhomogeneous materials. The goal of these investigations is to extend the capabilities of ultrasound in nondestructive evaluation of lossy, dispersive inhomogeneous media.

III. ULTRASONIC DETERMINATION OF ELASTIC CONSTANTS FOR HEXAGONAL MEDIA

Sound propagation in media with hexagonal symmetry can be characterized by five independent constants. These constants can be accurately determined by the measurement of five independent ultrasonic velocities. Four of the five constants can be determined by measurement of waves propagating parallel or perpendicular to the six-fold axis. Determination of the fifth elastic constant requires propagation of a wave at an angle with respect to the six-fold axis. In this Progress Report, we examine the error analysis for determination of this fifth elastic constant from measurement of a velocity propagating at an arbitrary angle with respect to the six-fold axis. We show that for media with a high degree of longitudinal anisotropy such as graphite fiber-reinforced epoxy improvement in accuracy may be obtained by propagation at an angle other than the conventional choice of forty-five degrees. Expressions for determination of the optimal angle are presented.

Elastic constants of fiber-reinforced composites are known only approximately. Unlike the case of many naturally occurring crystalline materials, it is not usually possible to specify a single set of elastic constants for a class of composites. Composites designated by the same generic name (e.g., graphite-epoxy) exhibit a range of values for the elastic constants. These values depend upon the characteristics of the fiber, the

PANEL b)

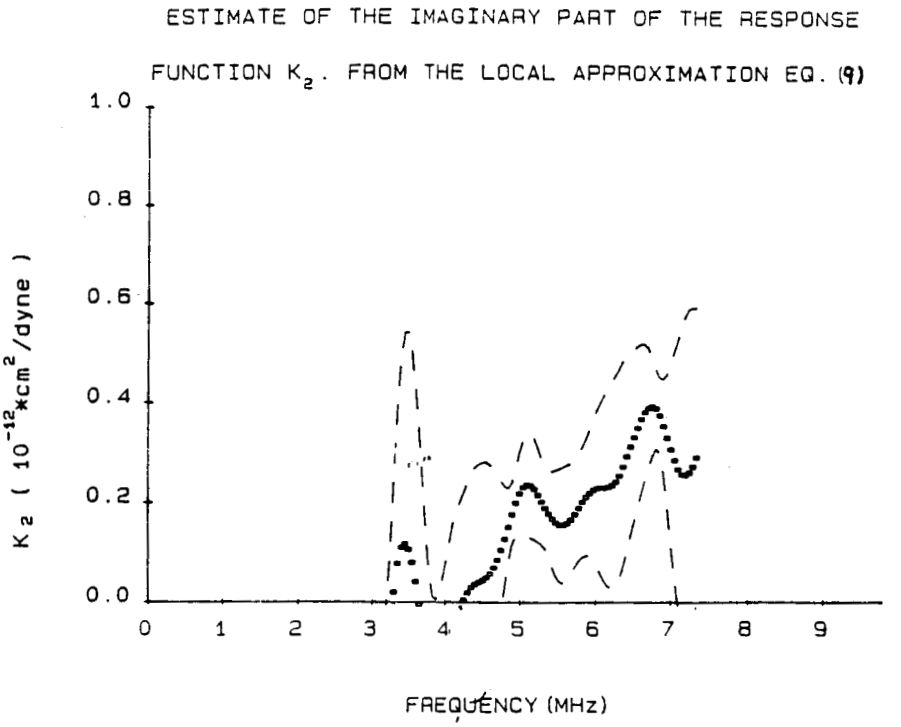

PANEL a)

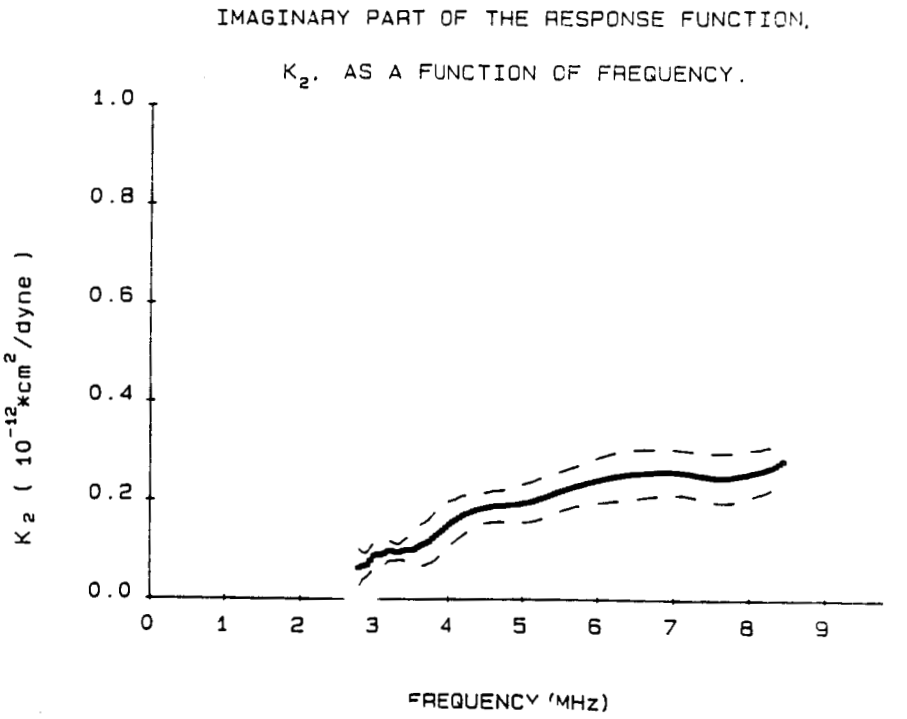

Figure 5 - Uniaxial graphite-epoxy insonified perpendicular to the fibers. In panel a) is an estimate of $K_2(\omega)$ based on experimentally obtained values of $K_1(\omega)$ and the local approximation (Eq.(9)). In panel b) the value of $K_2(\omega)$ derived directly from the experimental data. Both curves agree to within their error bars which are represented by dashed lines. The sample thickness is 3cm.

matrix, their relative proportions, and related manufacturing parameters. In this Progress Report we discuss wave propagation in hexagonal media (e.g., in graphite-epoxy composites) as an approach to the determination of elastic constants and hence material properties.

A. PHASE VELOCITY EQUATIONS FOR WAVE PROPAGATION IN A MERIDIAN PLANE

In the Progress Report covering the period September 15, 1985 through March 14, 1986 we discussed wave propagation in hexagonal media. Graphite-epoxy composites layed-up in a hexagonal close-packed (hcp) arrangement exhibit hexagonal symmetry and are thus *transversely isotropic;* that is, all material properties are independent of rotation about the stiff axis (i.e., fiber axis). Therefore, we can study the entire phase velocity surface by examining wave propagation in a meridian plane, which is any plane which includes the six-fold axis of symmetry.

The matrix of elastic constants [C_{ij}] for hexagonal media with the six-fold axis aligned along the x_1 axis (in the notation of the composites literature) and for wave propagation in a meridian plane is

$$[C_{ij}] = \begin{bmatrix} C_{11} & C_{12} & C_{12} & 0 & 0 & 0 \\ C_{12} & C_{22} & C_{23} & 0 & 0 & 0 \\ C_{12} & C_{23} & C_{22} & 0 & 0 & 0 \\ 0 & 0 & 0 & \frac{C_{22}-C_{23}}{2} & 0 & 0 \\ 0 & 0 & 0 & 0 & C_{55} & 0 \\ 0 & 0 & 0 & 0 & 0 & C_{55} \end{bmatrix} .$$

The analytic expressions for the phase velocities in a meridian plane, using ψ as the angle between the wave vector **k** and the six-fold axis of symmetry, are as follows.

The phase velocity for the pure shear mode is

$$V_S = \left[\frac{(C_{22} - C_{23})\sin^2\psi + 2C_{55}\cos^2\psi}{2\rho} \right]^{1/2} . \tag{22}$$

The quasi-shear phase velocity is

$$V_{qS} = \left[\frac{C_{22}\sin^2\psi + C_{11}\cos^2\psi + C_{55} - C_q}{2\rho} \right]^{1/2} \tag{23}$$

and the quasi-longitudinal phase velocity is

$$V_{qL} = \left[\frac{C_{22}\sin^2\psi + C_{11}\cos^2\psi + C_{55} + C_q}{2\rho} \right]^{1/2} , \tag{24}$$

where we have set

$$C_q \equiv \sqrt{[(C_{22} - C_{55})\sin^2\psi + (C_{11} - C_{55})\cos^2\psi]^2 + [(C_{12} + C_{55})^2 - (C_{22} - C_{55})(C_{11} - C_{55})]\sin^2 2\psi} .$$

The symbol ρ represents the combined (fiber plus matrix) density of the graphite-epoxy sample.

B. MEASUREMENT OF HEXAGONAL CONSTANTS

Since a medium with hexagonal symmetry is characterized by five independent elastic constants, we must measure at least five independent velocities to determine the full set of constants. Four of the elastic constants are easily determined.

For propagation parallel to the six-fold axis, the expressions for the phase velocities given in Equations (22) through (24) reduce to simple forms. The velocity of the longitudinal mode ($V_L^{\parallel}$) provides the stiffness of the six-fold axis

$$C_{11} = \rho \left[V_L^{\parallel} \right]^2 \tag{25}$$

with fractional error given by

$$\left[\frac{\sigma_{C_{11}}}{C_{11}} \right]^2 = 4 \left[\frac{\sigma_{V_L^{\parallel}}}{V_L^{\parallel}} \right]^2 . \tag{26}$$

The shear velocities ($V_S^{\parallel}$) are degenerate for propagation parallel to the six-fold axis, thus

propagation of a shear wave of arbitrary polarization provides

$$C_{55} = \rho \left[V_S^{\parallel} \right]^2 \tag{27}$$

with fractional error given by

$$\left[\frac{\sigma_{C_{55}}}{C_{55}} \right]^2 = 4 \left[\frac{\sigma_{V_S^{\parallel}}}{V_S^{\parallel}} \right]^2 . \tag{28}$$

C_{55} can also be determined by propagation perpendicular to the six-fold axis. The velocity of the shear mode which is polarized parallel with the six-fold axis (denoted by $V_{S_{\parallel}}^{\perp}$)(see the quasi-shear mode of Equation (22) with $\psi = 90°$) provides

$$C_{55} = \rho \left[V_{S_{\parallel}}^{\perp} \right]^2 \tag{29}$$

with fractional error similar to the expression in Equation (28). The symmetry represented by Equations (27) and (29) is an example of the well-known result[4] that one obtains the same value for the phase velocity under an exchange of the propagation and polarization directions.

The longitudinal mode propagating perpendicular to the six-fold axis ($V_L^{\perp}$) supplies the transversely isotropic longitudinal elastic constant, C_{22}, via

$$C_{22} = \rho \left[V_L^{\perp} \right]^2 \tag{30}$$

with fractional error given by

$$\left[\frac{\sigma_{C_{22}}}{C_{22}} \right]^2 = 4 \left[\frac{\sigma_{V_L^{\perp}}}{V_L^{\perp}} \right]^2 . \tag{31}$$

The other shear mode propagating perpendicular to the six-fold axis is polarized perpendicular to the six-fold axis (denoted by $V_{S_{\perp}}^{\perp}$). Measurement of this velocity provides C_{44}, which is $(C_{22} - C_{23})/2$. Thus, using C_{22} from Equation (22), we determine the fourth elastic constant C_{23},

$$C_{23} = C_{22} - 2\rho \left[V_{S_{\perp}}^{\perp} \right]^2 \tag{32}$$

with total error given by

$$\sigma_{C_{23}}{}^2 = \sigma_{C_{22}}{}^2 + 16\rho^2 V_{S_{\perp}}^{\perp}{}^2 \sigma_{V_{S_{\perp}}^{\perp}}{}^2 . \tag{33}$$

The remaining elastic constant represents a "matrix-fiber" interaction in a composite material. In the notation we are using, the fifth elastic constant is C_{12}. Inspection of the

velocity Equations (22-24) shows that the pure shear mode is independent of this constant. In addition, the quasi-longitudinal and quasi-shear modes are independent of this constant for two special angles, $\psi = 0°$ and $\psi = 90°$. Thus, we can determine this constant only by measurement of a quasi-longitudinal or quasi-shear velocity for propagation neither parallel nor perpendicular to the six-fold axis.

The choice of the angle at which the measurement should be made appears to have been heavily influenced by a paper by H.J. McSkimin.[5] In that work he measured the five elastic constants of single crystal cobalt. At the time this paper was submitted (June 1954) McSkimin was apparently unaware that the phase velocity was known analytically for any angle ψ. The analytic solutions had been published by Seeger and Schöck[6] in 1953 and, independently, by M.J.P. Musgrave[7] in 1954. The phase velocities do reduce to fairly simple forms for $\psi = 45°$, which were obtainable without knowledge of the complete solution for any angle ψ. McSkimin obtained these forms from Cady's book on piezoelectricity.[8] Many other researchers have followed McSkimin's precedent[9,10] so that today $\psi = 45°$ is the usual choice for measuring C_{12}. However, our calculations suggest that 45° may not be the optimum choice, at least for graphite-epoxy composites.

One approach would be to perform a large number of velocity measurements, using many different angles with respect to the six-fold axis. From this over-determined set one would then obtain average estimates of all five elastic constants. However, preparation of so many samples is rarely feasible. Indeed, one would prefer to determine the value from a single measurement at some optimum angle.

Consider a sample cut as suggested in Figure 6, with opposing faces flat and parallel and with the six-fold axis at some angle ψ with respect to the surface normal. The direction of the wave vector will be perpendicular to the surface. The velocities of the quasi-longitudinal and quasi-shear modes are then given by the following equation in ψ and the elastic constants of Equations (23) and (24).

$$V^2_{\substack{qL \\ qS}} = \frac{a \pm \sqrt{a^2 - 4b + 4(C_{12}+C_{55})^2 \sin^2\psi\cos^2\psi}}{2\rho} \tag{34}$$

where for convenience we have set

$$a \equiv C_{22}\sin^2\psi + C_{11}\cos^2\psi + C_{55} \tag{35}$$

and

$$b \equiv (C_{11}\cos^2\psi + C_{55}\sin^2\psi)(C_{22}\sin^2\psi + C_{55}\cos^2\psi) \quad . \tag{36}$$

Equation (34) can be inverted, to obtain an expression for the desired elastic constant,

Uni-axial Graphite Epoxy Sample

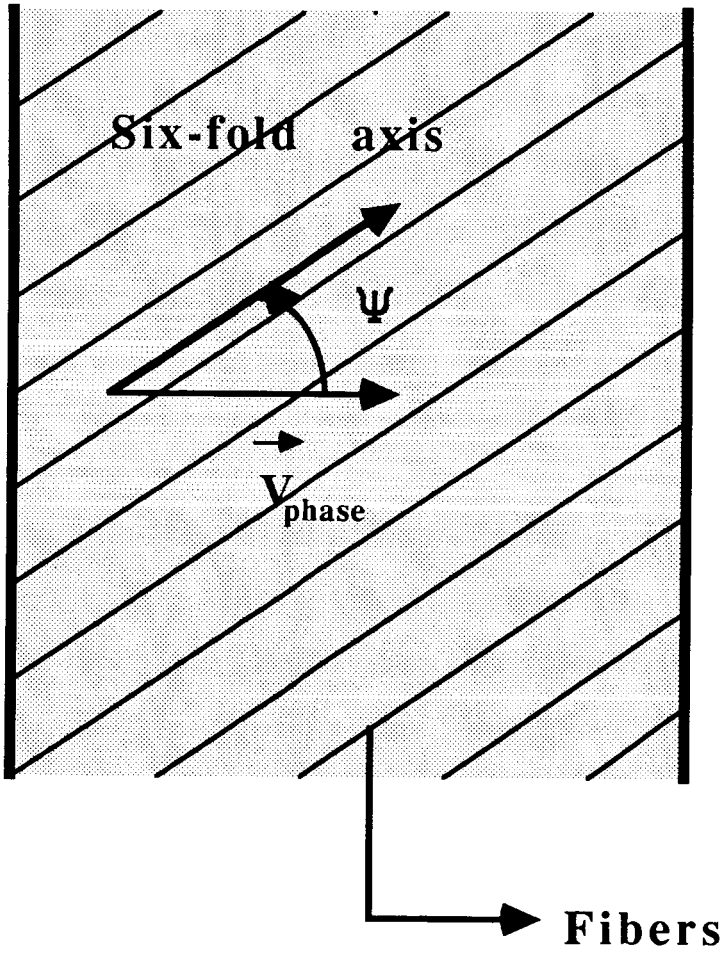

Figure 6 - Geometry of Sample

C_{12}, as

$$C_{12} = \frac{\sqrt{b - a\rho V^2 + \rho^2 V^4}}{|\sin\psi|\,|\cos\psi|} - C_{55} \quad . \tag{37}$$

Here a positive sign was chosen when taking the square root appearing in the numerator of the first term, so that C_{12} may be positive. We note that there is an interrelationship between the quasi-longitudinal and the quasi-shear velocities. In Equation (37), V represents the velocity of either mode. This seeming ambiguity arose in the derivation of Equation (37). At one point in the derivation, all the dependence on velocity (either mode) is contained in a single term. At that point, we have

$$\left[a - 2\rho V^2\right]^2 = \left\{ \begin{array}{c} \textit{terms independent of} \\ \textit{mode chosen} \end{array} \right\} \quad . \tag{38}$$

For the quasi-longitudinal mode, $[a - 2\rho V_{qL}^2]$ is less than zero, while for the quasi-shear mode that same term is greater than zero by the same amount. Squaring the term removes the difference in sign, so that Equation (37) is "independent" of the mode chosen.

We now have a measurement of the fifth elastic constant, obtained at some angle ψ. To make an estimate of the uncertainties in this result, we apply simple propagation of errors,[11,12] neglecting any uncertainty in the density as being relatively unimportant, and assuming no cross-correlations.[13] The uncertainty in C_{12} is given by

$$\sigma_{C_{12}}^2 = \left[\frac{\partial C_{12}}{\partial V}\right]^2 \sigma_V^2 + \left[\frac{\partial C_{12}}{\partial C_{11}}\right]^2 \sigma_{C_{11}}^2 + \left[\frac{\partial C_{12}}{\partial C_{22}}\right]^2 \sigma_{C_{22}}^2 + \left[\frac{\partial C_{12}}{\partial C_{55}}\right]^2 \sigma_{C_{55}}^2 \quad . \tag{39}$$

This result is quite general, and is useful despite the apparent complexity,

$$\sigma_{C_{12}} = \frac{1}{2|\sin\psi|\,|\cos\psi|\,\sqrt{b - a\rho V^2 + \rho^2 V^4}} \left\{ [4\rho^2 V^3 - 2a\rho V]^2 \sigma_V^2 \right. \tag{40}$$

$$+ [C_{22}\sin^2\psi\cos^2\psi + c_{55}\cos^4\psi - \rho V^2\cos^2\psi]^2 \sigma_{C_{11}}^2$$

$$+ [C_{11}\sin^2\psi\cos^2\psi + c_{55}\sin^4\psi - \rho V^2\sin^2\psi]^2 \sigma_{C_{22}}^2$$

$$\left. + [C_{22}\sin^4\psi + 2C_{55}\sin^2\psi\cos^2\psi + C_{11}\cos^4\psi - \rho V^2 - 2|\sin\psi|\,|\cos\psi|\,\sqrt{b - a\rho V^2 + \rho^2 V^4}]^2 \sigma_{C_{55}}^2 \right\}^{1/2}$$

where $\sigma_{C_{11}}$, $\sigma_{C_{22}}$, and $\sigma_{C_{55}}$ are given by Equations (26), (31), and (28), respectively.

In order to proceed let us assume that the fractional error in measuring any velocity is approximately constant for all desired measurements. Equation (40) can then be written as proportional to the fractional error in the velocity, with a complicated proportionality constant which depends on the measured elastic constants. For comparison with a simpler case, the proportionality constant is simply equal to 2 in Equations (26), (28), and (31).

We can easily evaluate the resulting expression numerically. In this Progress Report, we will use a set of elastic constants reported by Kriz and Stinchcomb,[9] for type AS-3501 graphite-epoxy, as input values to our equations. These constants are summarized below.

$$C_{11} = 16.1 \quad X\ 10^{10}\ \frac{N}{m^2}$$

$$C_{12} = 0.650\ X\ 10^{10}\ \frac{N}{m^2}$$

$$C_{22} = 1.45\ X\ 10^{10}\ \frac{N}{m^2}$$

$$C_{23} = 0.724\ X\ 10^{10}\ \frac{N}{m^2}$$

$$C_{55} = 0.710\ X\ 10^{10}\ \frac{N}{m^2}$$

Figure 7 presents the estimated fractional error in C_{12}, calculated as a function of the angle between the surface normal and the fibers, assuming a five per cent fractional error in the measurements of the velocities. Since the velocities are independent of C_{12} at $\psi = 0°$ and $\psi = 90°$, Equation (40) diverges as expected as those angles are approached. The overall magnitude of the fractional error is quite large, with the minimum uncertainty on the order of one hundred per cent. Thus we note that the fifth elastic constant is indeed difficult to determine precisely.

One significant feature of Figure 7, summarized in bar graph fashion in Figure 8, is that the minimum error (i.e., minima in $\sigma_{C_{12}}$) lies far from the traditional measurement angle of 45°. Indeed, for this material one can achieve an improvement in precision of more than a factor of two by measuring near $\psi = 77°$ rather than at $\psi = 45°$. We note that the location of this optimum angle is a function of C_{12}, the very quantity we are striving to measure. Fortunately, the location of the minimum exhibits a fairly weak dependence on C_{12}, so that a rough estimate of C_{12} will permit the experimenter to make an improved determination of C_{12} relatively close to the optimum angle. We suggest that there may be similar "optimum angles" for other hexagonal materials, so that

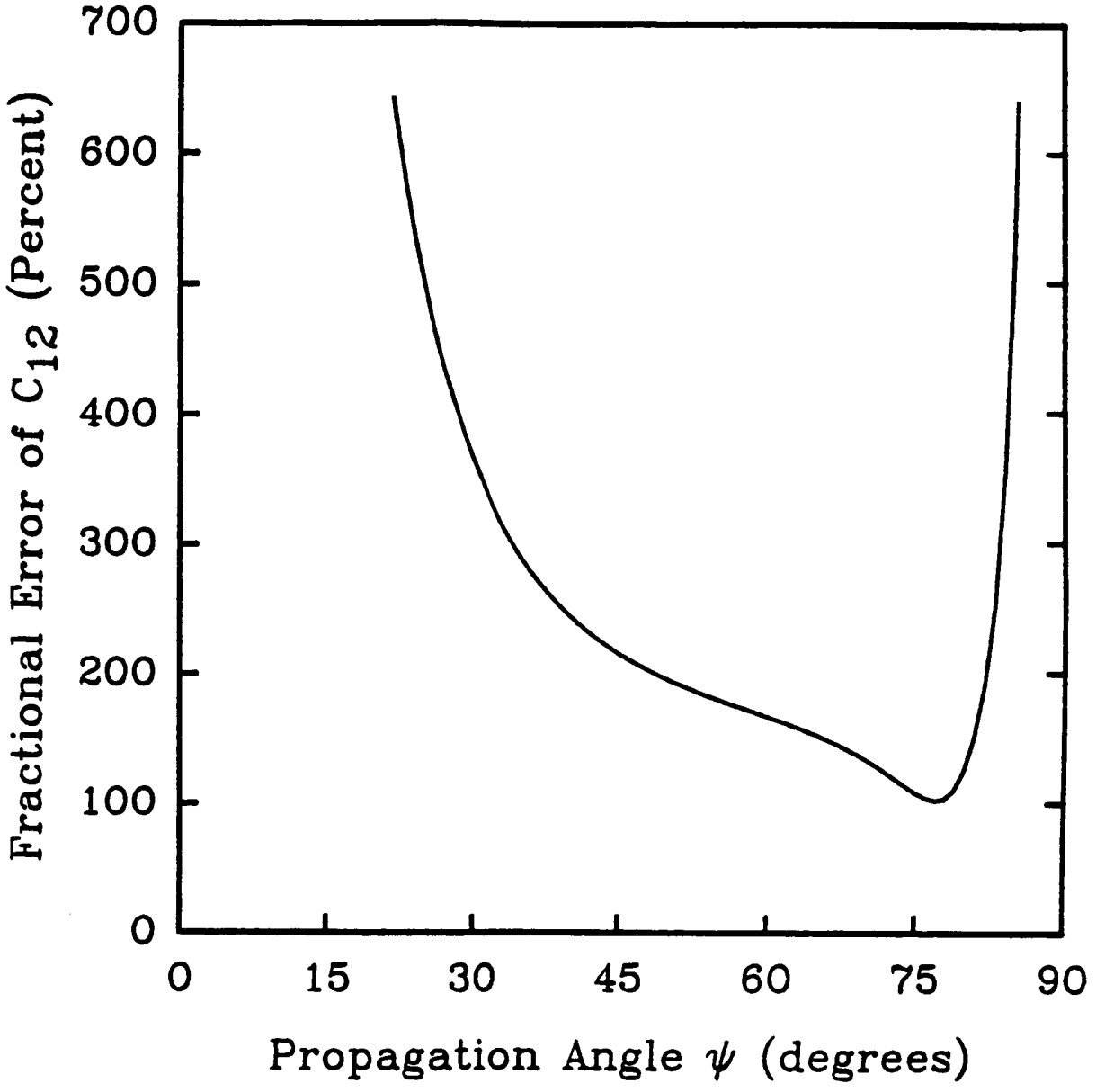

Figure 7 - Fractional error in determination of C_{12} as a function of the angle at which the measurement was made relative to the fiber axis. A uniform fractional error of five percent in the measurement of all velocities was assumed.

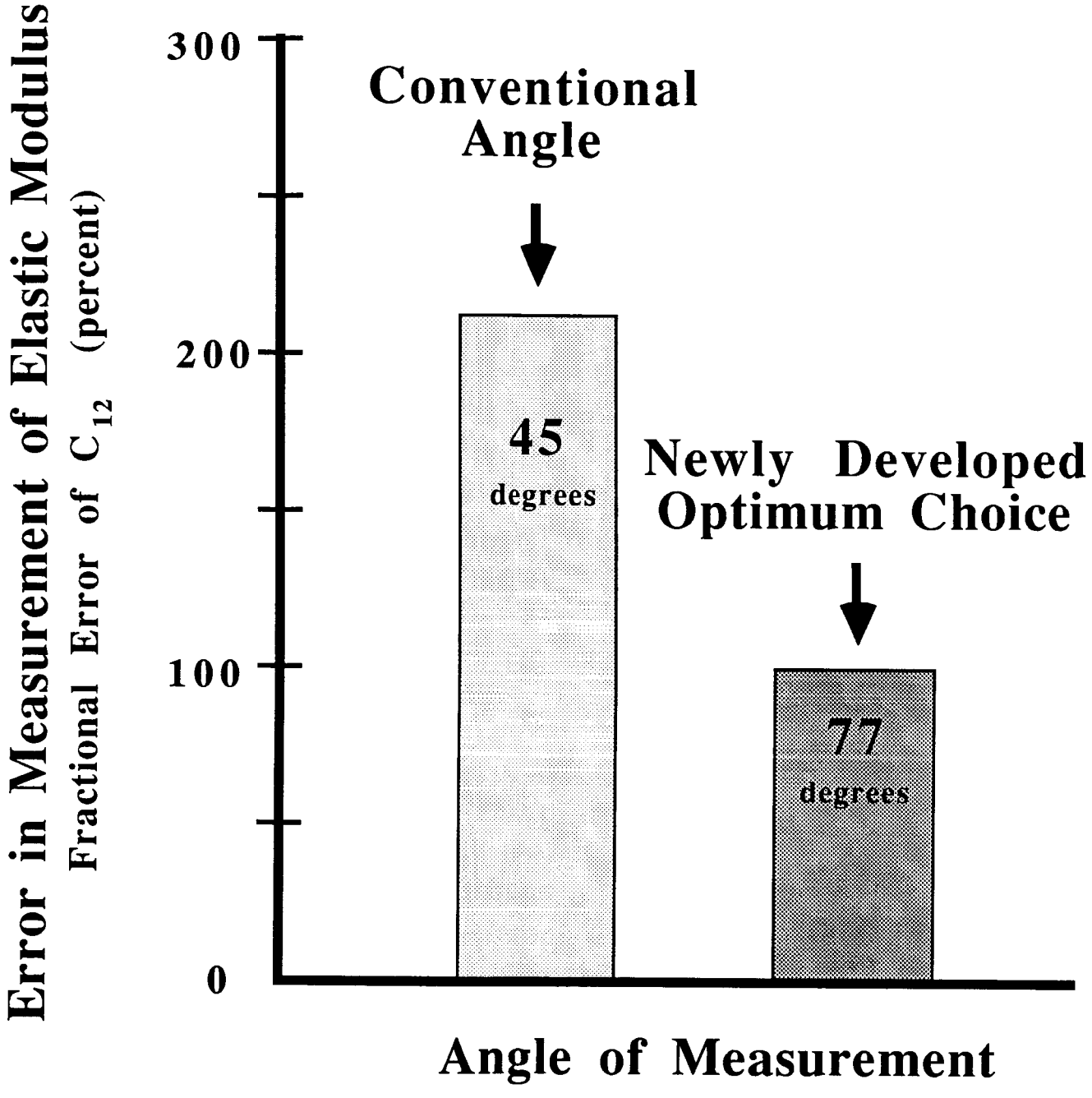

Figure 8 - Comparison of the Fractional Error in the measurement of C_{12} between the conventional angle (45°) and the predicted optimum angle (77°).

consideration of the type of calculations made here may prove more generally useful.

References

1. M. O'Donnell, E.T. Jaynes, and J.G. Miller, "General Relationships Between Ultrasonic Attenuation and Dispersion," *J. Acoust. Soc. Am.*, vol. 63, pp. 1935-1937, 1978.
2. M. O'Donnell, E.T. Jaynes, and J.G. Miller, "Kramers-Kronig Relationship Between Ultrasonic Attenuation and Phase Velocity," *J. Acoust. Soc. Am.*, vol. 69, pp. 696-701, 1981.
3. W. Sachse and Y.H. Pao, *Journal of Applied Physics*, vol. 49, pp. 4320-4327, 1978.
4. B.A. Auld, *Acoustic Fields and Waves in Solids, Vol I,* Wiley Interscience, New York, 1973.
5. H.J. McSkimin, "Measurement of the Elastic Constants of Single Crystal Cobalt," *J. Appl. Phys.*, vol. 26, pp. 406-409, 1955.
6. A. Seeger and G. Schöck, "Die Aufspaltung von Versetzungen in Metallen Dichtester Kugelpackung," *Acta. Metall.*, vol. 1, pp. 519-530, 1953.
7. M.J.P. Musgrave, "On the Propagation of Elastic Waves in Aeolotropic Media II. Media of Hexagonal Symmetry," *Proc. Roy. Soc.*, vol. 226, pp. 356-366, 1954.
8. W.G. Cady, *Piezoelectricity,* McGraw-Hill, New York, 1946.
9. R.D. Kriz and W.W. Stinchcomb, "Elastic Moduli of Transversely Isotropic Graphite Fibers and Their Composites," *Exp. Mech.*, vol. 19, pp. 41-49, 1979.
10. D.I. Bolef, N.T. Melamed, and M. Menes, "Elastic Constants of Hexagonal Cadmium Sulfide," *J. Phys. Chem. Solids*, vol. 17, pp. 143-148, 1960.
11. Philip R. Bevington, *Data Reduction and Error Analysis for the Physical Sciences,* McGraw-Hill, New York, 1969.
12. John R. Taylor, *An Introduction to Error Analysis,* University Science Books, Mill Valley, CA, 1982.
13. John R. Taylor, "Simple Examples of Correlations in Error Propagation," *Am. J. Phys.*, vol. 53, pp. 663-667, 1985.